5. Two-layer Flows in Rotating Channels.

The exchange flow between a marginal sea or estuary and the open ocean is often approximated using two-layer stratification. Two-layer models are most convincing when the interfacial region separating the upper and lower fluids is relatively thin. The exchange flow in the Strait of Gibraltar exhibits this behavior, at least at certain locations and times (Figure I9). The vertical density and velocity profiles taken near the Camerinal Sill show a relatively sharp transition between slab-like upper and lower water masses. Elsewhere, the Gibraltar interface can be thicker and can contribute significantly to the overall mass budget for the strait. The Bab al Mandab (BAM) exchange flow experiences variations throughout the water column that are quite continuous (Figures 1.10.7 and 5.0.1). Under such conditions, a two-layer model might still give guidance provided that motions over the water column are associated with the lowest internal mode of the stratified shear flow.

Rotational effects are often ignored in applications such as Gibraltar and the BAM, where the narrowest widths are about the same or less than the internal Rossby radius of deformation based on the local depth scale. However valid this assumption is, it certainly fails where the strait broadens into the neighboring marginal sea or ocean. For most deep-ocean overflows rotation is paramount but exchange dynamics are less important. However, the overflow itself is often composed of fluid drawn from an intermediate water mass in the upstream basin, with a weaker contribution from deep waters. The deep and intermediate water masses may exhibit independent behavior that might be captured by treating the two as separate homogeneous layers. The flow of Antarctic Bottom Water through the Vema Channel (Figure 5.0.2) provides an example. Upstream of the sill (right-hand section), the deep isopycnals slope downwards from left to right, or west-to-east. Slightly downstream of the sill section (middle frame), the slopes in the deepest (dark shaded) water are reversed and slope upwards. Isopycnals on the right-hand side of the Channel become pinched together as a result. Further downstream the deep isotherms regain their original slope (left-hand frame).

The early sections in the chapter provide a review of two-layer hydraulic phenomena in nonrotating systems. Much of this subject is covered in Baines (1995); our review concentrates on maximal exchange, overmixing, and other concepts that arise in the consideration of ocean exchange flow and that have not been emphasized in other texts. The final sections explore the difficult and nascent field of two-layer hydraulics with rotation.

Figure Captions

5.0.1 April 1996 CTD cast at the Bab al Mandab sill along with a March 1996 average velocity profile (from ADCP). (From Pratt et al. 1999, Figure 6).

5.0.2 Three cross sections of the Vema Channel showing depths of selected potential density(σ_4) surfaces. Sections 1 is upstream of the sill, Section 4 is close to the sill, and Section 6 is downstream of the sill. (From Hogg, 1983).

5.1 Formulation of two-layer, semigeostrophic models.

The channel is laid out as before, with a rectangular cross-section and width and bottom elevations w^* and h^* (Figure 5.1.1). Two homogeneous layers of fluid are now present and we follow the oceanographic convention in numbering the top and bottom layers 1 and 2 respectively. The density ρ_2 of the bottom layer is only slightly greater than ρ_1.

In formulating the governing equations, we will employ a number of standard approximations. The first involves the treatment of the upper boundary of the two-fluid system. If this boundary were a free surface, overlain by a vacuum or by a substantially less dense fluid such as air, then free surface gravity waves would exist. In nearly all oceanographic applications the propagation speeds of these waves are much greater than the typical fluid velocities. In the Denmark Strait overflow, for instance, typical peak velocities are about 1m/s whereas the speeds of long, free surface gravity waves are up to 100 times larger. The Froude number $F_d = v^* / \sqrt{gd^*}$ based on free surface dynamics is therefore <<1. Our previous experience with homogeneous flows suggests that it is unlikely that bottom topography (or width variations) will cause significant departures of the free surface elevation from a horizontal plane. In fact, the free surface elevation z_T^* can be shown to obey

$$\frac{dz_T^*}{dy^*} \approx F_d^2 \left(\frac{d^*}{w^*} \frac{dw^*}{dy^*} - \frac{dh^*}{dy^*} \right),$$

obtained by rearrangement of Equation (1.4.3) with F_d<<1. Thus, when F_d is small, the departure in the free surface elevation is smaller by a factor F_d^2 than the variations in w or h. For the Denmark Strait, F_d^2 is about 10^{-4}. On the other hand, the speeds of the *internal* waves that propagate on the interface between the two layers are much smaller and the associated Froude numbers much larger. One might expect, then, that the typical vertical excursions of the interface will be much greater than those of the free surface. Since the latter now give a negligible contribution to variations in the upper layer depth, we simply regard the upper surface as rigid and horizontal. If $z^*=z_T^*$ denotes the constant elevation of this surface, h^* the bottom elevation, and d_1^* and d_2^* the thicknesses of the two layers, then

$$z_T^* = h^* + d_2^* + d_1^* .$$

The rigid lid approximation is explored more formally in Exercise 1.

Under the assumption that variations in the horizontal are gradual on the scale of the depth, the pressures in each layer will be hydrostatic. Therefore

$$p_1^* = p_T^* + \rho_1 g(z_T^* - z^*) \tag{5.1.1}$$

and

$$\begin{aligned} p_2^* &= p_T^* + \rho_1 g(z_T^* - h^* - d_2^*) + \rho_2 g(h^* + d_2^* - z^*) \\ &= p_T^* + g(\rho_2 - \rho_1)(h^* + d_2^*) + g(\rho_1 z_T^* - \rho_2 z^*) \end{aligned}, \tag{5.1.2}$$

where $p_T^*(x^*,y^*,t^*)$ denotes the pressure at the rigid upper lid.

There are two other standard assumptions. The first is that the channel geometry varies only gradually along its axis, suggesting that the along-channel velocity v_i^* is geostrophically balanced. The formal arguments leading to this 'semigeostrophic' approximation are essentially those laid out in Chapter 2. The second assumption is that the density difference between the two layers is relatively small: $\Delta\rho / \overline{\rho} = (\rho_2 - \rho_1) / [\frac{1}{2}(\rho_2 + \rho_1)] << 1$. This is the basis for the Boussinesq approximation, in which the actual density ρ_1 or ρ_2 is replaced by a representative value such as the average $\overline{\rho}$, except where they are multiplied by g. The reasoning here is that g is much larger than accelerations of the fluid itself, and its product with the small $\Delta\rho / \overline{\rho}$ is nonneglegible. The semigeostrophic equations governing the inviscid, Boussinesq, two-fluid system are then

$$f v_1^* = \frac{1}{\overline{\rho}} \frac{\partial p_T^*}{\partial x^*} \tag{5.1.3}$$

$$\frac{\partial v_1^*}{\partial t^*} + u_1^* \frac{\partial v_1^*}{\partial x^*} + v_1^* \frac{\partial v_1^*}{\partial y^*} + f u_1^* = -\frac{1}{\overline{\rho}} \frac{\partial p_T^*}{\partial y^*} \tag{5.1.4}$$

$$f v_2^* = \frac{1}{\overline{\rho}} \frac{\partial p_T^*}{\partial x^*} + g' \frac{\partial d_2^*}{\partial x^*} \tag{5.1.5}$$

$$\frac{\partial v_2^*}{\partial t^*} + u_2^* \frac{\partial v_2^*}{\partial x^*} + v_2^* \frac{\partial v_2^*}{\partial y^*} + f u_2^* = -\frac{1}{\overline{\rho}} \frac{\partial p_T^*}{\partial y^*} - g' \left(\frac{\partial d_2^*}{\partial y^*} + \frac{\partial h^*}{\partial y^*} \right) \tag{5.1.6}$$

where $g' = \Delta\rho g / \overline{\rho}$ is the reduced gravity.

The equation of mass conservation within layer i is

$$\frac{\partial d_i^*}{\partial t^*} + \frac{\partial (u_i^* d_i^*)}{\partial x^*} + \frac{\partial (v_i^* d_i^*)}{\partial y^*} = 0 \tag{5.1.7}$$

If (5.1.5) is subtracted from (5.1.3) the result is the *thermal wind* relation for the along-channel velocity component:

$$f(v_1^* - v_2^*) = -g' \frac{\partial d_2^*}{\partial x^*}. \qquad (5.1.8)$$

The difference in velocities between the two layers is thus proportional to the cross-channel slope of the interface.

The semigeostrophic potential vorticity within layer *i* is defined by

$$q_i^* = \frac{f + \frac{\partial v_i^*}{\partial x^*}}{d_i^*}, \qquad (5.1.9)$$

and conservation of this property following the fluid motion,

$$\left(\frac{\partial}{\partial t^*} + u_i^* \frac{\partial}{\partial x^*} + v_i^* \frac{\partial}{\partial y^*} \right) q_i^* = \frac{d_i^* q_i^*}{dt^*} = 0 ,$$

may be shown in the same manner as for a homogeneous fluid.

In the event the potential vorticity is uniform within each layer, it is convenient to write

$$q_i^* = \frac{f}{D_{i\infty}} \qquad (5.1.10)$$

where $D_{i\infty}$ represents the potential depth of layer *i*. Using the above definition in (5.1.9) and combining the two results with (5.1.8) leads to an equation for the cross-channel structure of the flow

$$\frac{\partial^2 d_2^*(x^*, y^*, t^*)}{\partial x^{*2}} - L_I^{-2} d_2^*(x^*, y^*, t^*) = -\frac{f^2 (z_T^* - h^*)}{g' D_{1\infty}} \qquad (5.1.11)$$

where

$$L_I = \left[\frac{g' D_{1\infty} D_{2\infty}}{f^2 (D_{1\infty} + D_{2\infty})} \right]^{1/2} \qquad (5.1.12)$$

is the internal Rossby radius of deformation. Equation (5.1.11), which is similar to the cross-channel structure equation (2.2.2) governing the single-layer case, shows that the interface will have a boundary layer structure with *e*-folding scale L_I when the channel width is >> L_I. Through the thermal wind relation this structure will be imposed on the shear velocity v_1^*-v_2^*. However, v_1^* and v_2^* need not individually decay away from the sidewalls.

When the flow is steady, individual transport stream functions ψ_1^* and ψ_2^* can be defined such that

$$v_i^* d_i^* = \frac{\partial \psi_i^*}{\partial x^*}, \quad \text{and } u_i^* d_i^* = -\frac{\partial \psi_i^*}{\partial y^*}. \tag{5.1.13}$$

The semigeostrophic Bernoulli functions for each layer are conserved along their respective streamlines:

$$B_1^*(\psi_1^*) = \frac{v_1^{*2}}{2} + \frac{p_T^*}{\bar{\rho}} \tag{5.1.14}$$

and

$$B_2^*(\psi_2^*) = \frac{v_2^{*2}}{2} + \frac{p_T^*}{\bar{\rho}} + g'(d_2^* + h^*). \tag{5.1.15}$$

We leave it as an exercise to show

$$\frac{dB_i^*}{d\psi_i^*} = q_i^*. \tag{5.1.16}$$

In most problems it is convenient to eliminate the rigid lid pressure and work with quantities that govern the internal structure of the flow. For example, subtraction of (5.1.15) from (5.1.14) eliminates p_T^*, leaving

$$\Delta B^*(\psi_1^*, \psi_2^*) = B_2^*(\psi_2^*) - B_1^*(\psi_1^*) = \frac{v_2^{*2} - v_1^{*2}}{2} + g'(d_2^* + h^*). \tag{5.1.17}$$

The quantity ΔB is sometimes referred to as the internal energy (per unit mass). It should be stressed that ΔB^* is not conserved following ψ_1^* or ψ_2^* unless the two streamlines coincide, such as at a vertical boundary that extends through both layers.

Exercises:

1) Reformulate equations (5.1.3-5.1.7) to allow for a free upper surface (at which the pressure may assumed to be zero). Though inspection of these equations, formulate velocity, length and time scales based on the *internal* dynamics of the flow (i.e. use g' rather than g). Under this scaling, show that the contribution to d_1^* from a typical

displacement of the interface is much greater than the contribution from a typical displacement of the free surface. Deduce that the free surface displacement can be neglected in the continuity equation for the upper layer, so that the upper surface can effectively be treated as rigid.

2) Show that the Bernoulli functions as defined by (5.1.14) and (5.1.15) are indeed conserved along streamlines of the respective layers, provided that the flow is steady.

3) Prove (5.1.16).

4) Using the expression for linear wave speed of an internal disturbance in a nonrotating, two layer system (see 5.2.3) show that the two-layer Rossby radius of deformation (5.1.12) may be interpreted as the distance that such a wave will travel in a period $1/f$.

Figure Captions

5.1.1 Definition Sketches.

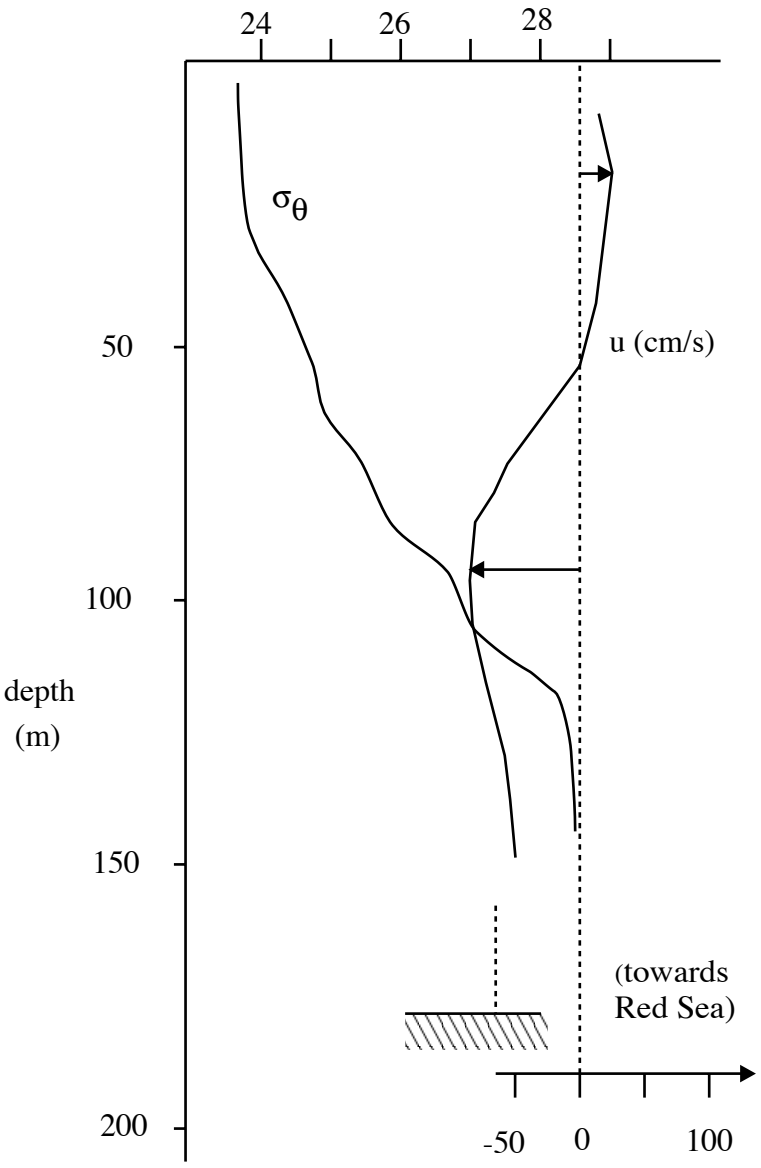

Figure 5.0.1

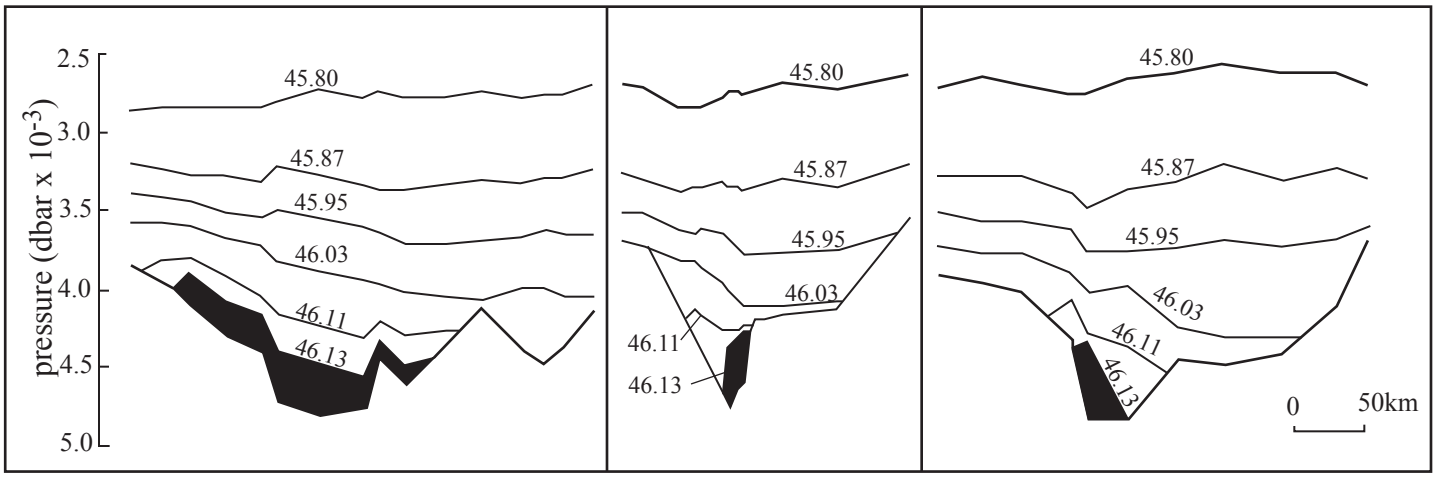

Section 6 Section 4 Section 1

Figure 5.0.2

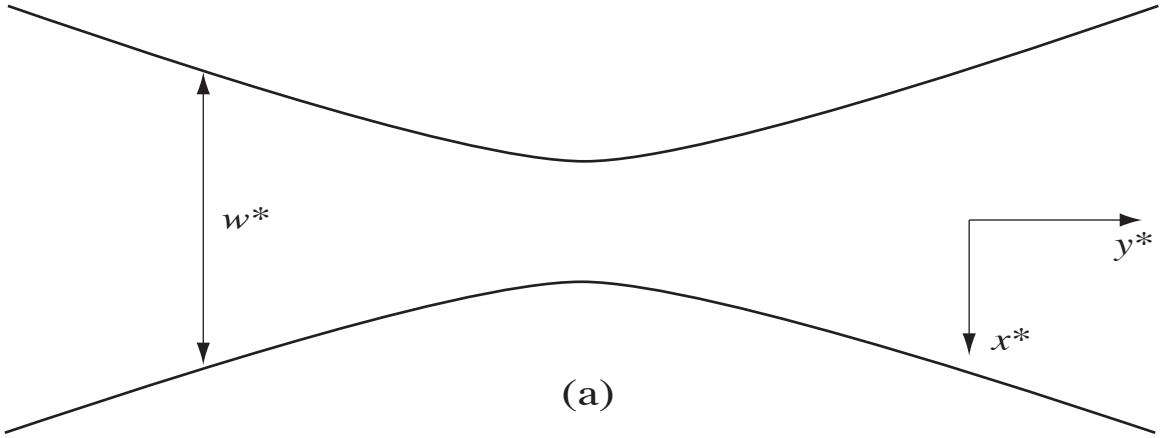

(a)

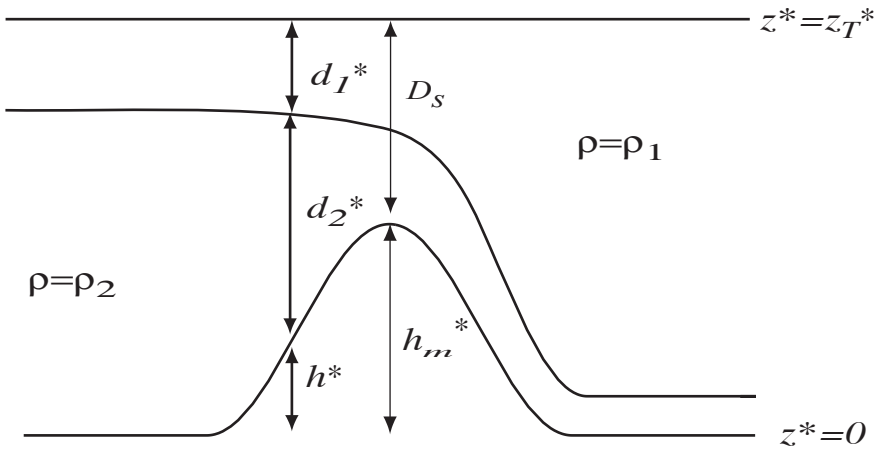

(b)

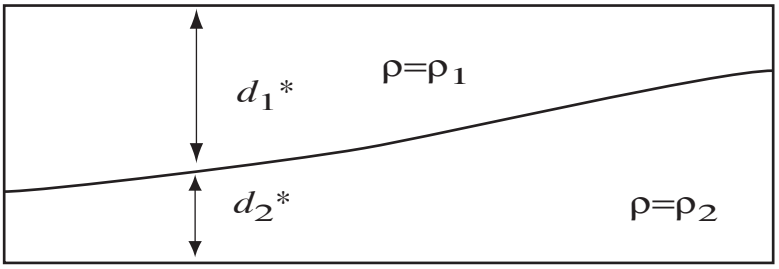

x*=-w*/2 x*=w*/2

(c)

Figure 5.1.1